Semnan University

Progress in Physics of Applied Materials

journal homepage: https://ppam.semnan.ac.ir/

Comparison of thermoelectric properties of armchair germanene nanoribbon and armchair germanene nanomesh

R. Kalami, S.A. Ketabi*

School of Physics, Damghan University, Damghan, Iran.

ARTICLE INFO

Article history:
Received: 28 November 2023
Revised: 12 December 2023
Accepted: 23 December 2023

Keywords:
Germanene
Quantum antidots
Seebeck coefficient
Figure of merit

ABSTRACT

This study investigates the thermoelectric properties of pristine armchair germanene nanoribbons (AGeNR) and those defected by quantum antidot arrays (AGeNM). The researchers employed a tight-binding model and the non-equilibrium Green's function formalism to conduct the study. AGeNM structures were created by introducing quantum antidot arrays in the form of symmetric and asymmetric rhomboid shapes in the central region of the pristine nanoribbons and their electrodes. The study reveals that different AGeNMs exhibit varying band gaps, influencing their electronic and thermoelectric behaviors. It is important to note that the presence of quantum antidot arrays introduces scattering of electrons and phonons in the nanoribbons, resulting in new thermoelectric properties such as the Seebeck coefficient, electrical conductance, electron and phonon thermal conductance, and ZT factor. The symmetry of the quantum antidot array shapes significantly influences the system's thermoelectric properties. The study paves the way for the development of more efficient nanoscale thermoelectric devices.

1. Introduction

Currently, the thermoelectric properties of nanoscopic systems have attracted a lot of attention. This is due to the potential to convert heat into electrical energy at the nanoscale in these systems [1-3]. The efficiency of a thermoelectric device is generally characterized by the figure of merit $ZT = \frac{S^2 GT}{K}$, where S is the Seebeck coefficient, G is the electronic conductance, T is the temperature, and K is the total thermal conductance, including contributions from both electrons and phonons. The ideal thermoelectric material has a high Seebeck coefficient S and a low thermal conductance K [4-6]. Both electrons and phonons play roles in the heat current. Hence, thermal conductance can be written as $K = K_e + K_{ph}$ [7, 8]. Therefore, decreasing the thermal conductance through increasing the scattering of phonon and electron can be one of the most promising ways to advance thermoelectric materials [9, 10]. The scattering of phonons and electrons, and consequently, figure of merit, can be enhanced via approaches such as synthesizing nanostructures and nanocomposites, and doping materials [9, 11-15]. Theoretical predictions [16] and experimental findings [17] have demonstrated that in comparison to bulk materials, low-dimensional or nanoscale systems can display much higher ZT values. This feature can result in a positive outlook for thermoelectric applications [18-20]. Furthermore, the presence of quantum antidots in different materials causes the scattering of electron and phonon-defect. As a consequence, the thermal conductance significantly decreases [21]. Quantum antidot arrays have been the issue of recent experimental research. These arrays with different geometries have been produced through various techniques [22]. Recently, quantum antidot lattices in graphene have attracted much attention [12]. This interest is due to the point that by generating an array of holes (quantum antidots) in the graphene layer, a band gap (which is essential for using graphene in transistor architectures) can be shaped. The size of the gap can be adjusted by changing the geometry of the quantum antidot shape, the size of the antidot shape, and the number of separated atoms [23]. Besides, in recent studies, the thermoelectric properties of two-dimensional graphene antidot lattices have been examined. This has resulted in

* Corresponding author.
E-mail address: saketabi@du.ac.ir

Cite this article as:
Kalami, R. and Ketabi S.A., 2023. Comparison of thermoelectric properties of armchair germanene nanoribbon and armchair germanene nanomesh. *Progress in Physics of Applied Materials*, *3*(2), pp.169-176. DOI: 10.22075/PPAM.2023.32472.1072

generating materials that have high *ZT*. It has also been shown that *ZT* can be enhanced through the creation of quantum antidots in the electrodes of graphene nanoribbons [6]. Graphene and germanene are common in their honeycomb lattice structures. However, the larger ionic radius of germanium, in comparison to carbon, causes the buckling of the lattice [23, 24]. Since, buckling has effects on the vibrational modes of germanene, phonon heat conduction decreases. Recently, researchers have become interested in the thermoelectric properties of germanene nanoribbons (GeNRs) owing to their quantum restrictions caused by buckling. This restriction can lead to a significant increase in the figure of merit in this structure [1]. Creating quantum antidots in such structures generates new quantum confinements. This issue can be promising for a material with a higher figure of merit [25]. The thermoelectric properties of GeNRs defected by quantum antidots have not been investigated as they deserve.

In this study, we utilize both the non-equilibrium Green's function (NEGF) method and the tight-binding model to compare the thermoelectric characteristics of two types of armchair germanene nanoribbons (AGeNR). The first type is a pristine AGeNR, while the second type is an AGeNR defected by quantum antidot arrays, also known as armchair germanene nanomesh (AGeNM). We design AGeNMs using quantum antidots in the shapes of symmetric and asymmetric rhomboids. We investigate the thermoelectric properties of both pristine AGeNR and AGeNMs. Our findings show that by introducing quantum antidots and adjusting the temperature appropriately, these AGeNMs can achieve remarkably high *ZT* values, indicating their potential for thermoelectric applications. We observe that the presence of quantum antidots in the germanene nanoribbon significantly reduces thermal conductance. Furthermore, we conclude that the existence of quantum antidot arrays enhances the Seebeck coefficient due to the quantum interference phenomenon within the system. These characteristics play a vital role in improving the thermoelectric efficiency factor and increasing the value of *ZT*. Therefore, by creating symmetric and asymmetric rhomboid quantum antidots, the thermoelectric behavior of AGeNRs can be improved through interference effects and the reduction of electron and phonon mean free path. The symmetry of the defects is an essential factor in modifying the thermoelectric properties of AGeNMs. When the quantum antidot arrays have symmetric shapes, their thermoelectric properties resemble those of pristine AGeNR. Thus, by considering the symmetry or asymmetry of the shape, the thermoelectric properties of the system can be adjusted.

The motivation of the present work is to explore the thermoelectric properties of nanoscopic systems, with a focus on AGeNR and their defected counterparts, AGeNM. The work is driven by the potential to convert heat into electrical energy at the nanoscale, which has garnered significant attention due to its implications for improving the efficiency of thermoelectric devices.

2. Model and the computational scheme

The top and side views of the molecular structure of armchair germanene are shown in Figure 1. In the present research, one armchair germanene nanoribbon with the width of N=11, connected to two semi-infinite electrodes, was considered. It has been presented in Figure 2, and Figure 3 illustrates the different configurations of quantum antidot arrays in the middle region of AGeNR and its electrodes with the width of *N*=11 considered in this study (AGeNMs). Different types of quantum antidot arrays displayed in these figures are symmetric and asymmetric rhomboid-type quantum antidot arrays.

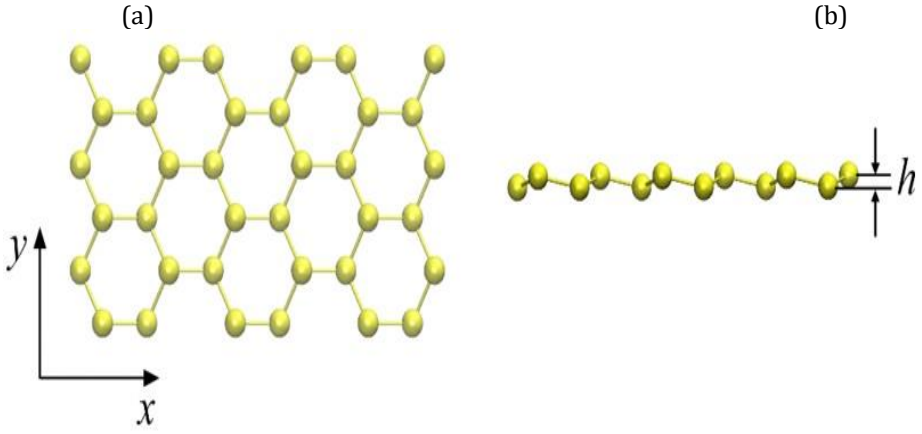

Fig. 1. (a) Top and (b) side view of armchair germanene molecular structure.

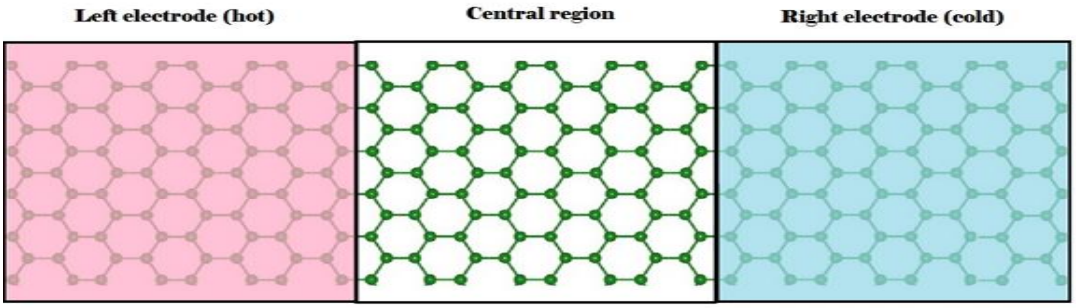

Fig. 2. The schematic view of armchair germanene nanoribbon with width of *N*=11 connected to two electrodes with hot and cold source.

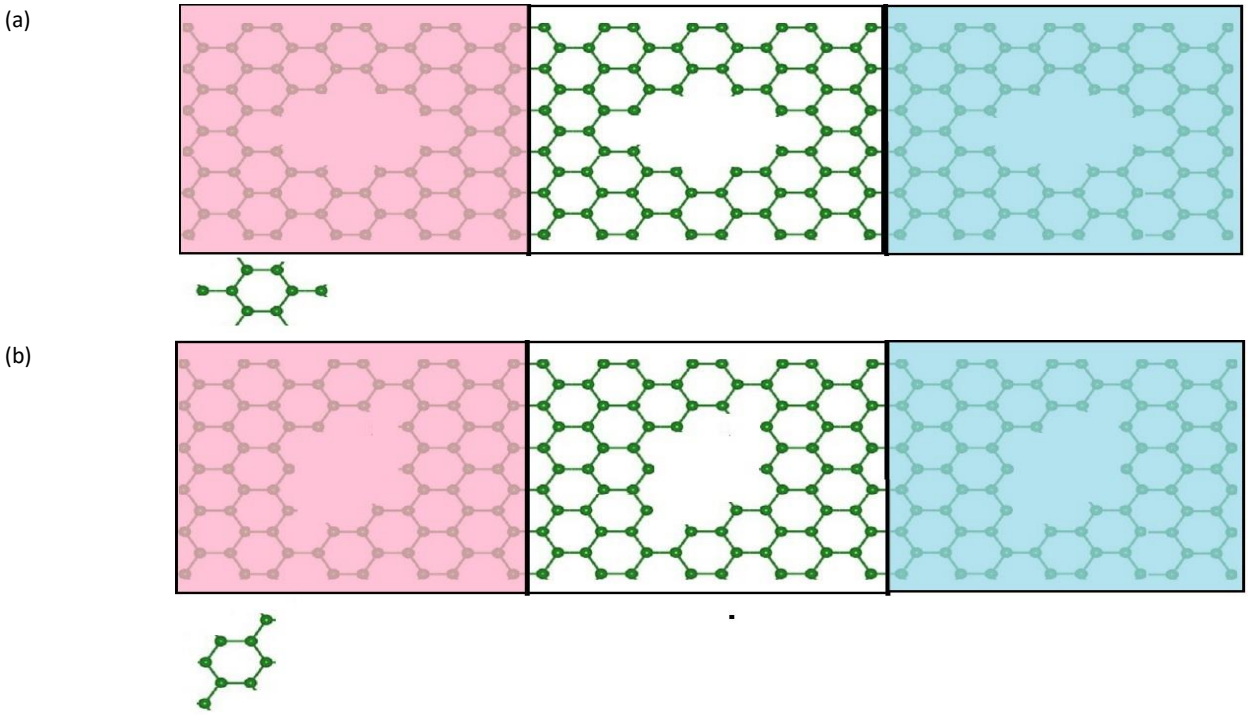

Fig. 3. The schematic view of nanoribbons of two different quantum antidot arrays with (a) symmetric rhomboid, and (b) asymmetric rhomboid topologies connected to two electrodes with hot and cold source.

To determine the thermoelectric properties of AGeNR and AGeNMs, the nearest-neighbor tight-binding (TB) model and the non-equilibrium Green's function (NEGF) formulation approach have been utilized [26-29]. Hamiltonian matrix for a typical junction such as the AGeNR and AGeNM model in terms of Hamiltonian sub-matrixes may be written as:

$$H = \begin{pmatrix} H_L & H_{LC} & 0 \\ H_{CL} & H_C & H_{CR} \\ 0 & H_{RC} & H_R \end{pmatrix} \quad (1)$$

Where $H_{L(R)}$ is a one-band tight-binding approximation description of the left (L) and right (R) electrodes. H_C, the Hamiltonian of the AGeNR and AGeNM, H_γ with $\gamma = L, R$ the Hamiltonian of left (right) electrode and $H_{C\gamma}$, the Hamiltonian of the coupling between the central surface and electrodes within the tight-binding model, have the following forms:

$$H = \varepsilon_0 \sum_i c_{i\alpha}^\dagger c_{i\alpha} + t \sum_{\langle i,j \rangle} c_{i\alpha}^\dagger c_{j\alpha} + i \frac{\lambda_{SO}}{3\sqrt{3}} \sum_{\langle\langle i,j \rangle\rangle} v_{ij} c_{i\alpha}^\dagger \sigma_{\alpha\beta}^z c_{j\beta} - i \frac{2}{3} \lambda_{Ra} \sum_{\langle\langle i,j \rangle\rangle \alpha\beta} \tau_{ij} c_{i\alpha}^\dagger (\vec{\sigma} \times \vec{d}_{ij}^{\,0})_{\alpha\beta}^z c_{j\beta} \quad (2)$$

$$H_{C\gamma} = t \sum_{\langle i,j \rangle} c_{i\alpha}^\dagger c_{j\alpha} + i \frac{\lambda_{SO}}{3\sqrt{3}} \sum_{\langle\langle i,j \rangle\rangle} v_{ij} c_{i\alpha}^\dagger \sigma_{\alpha\beta}^z c_{j\beta} - i \frac{2}{3} \lambda_{Ra} \sum_{\langle\langle i,j \rangle\rangle \alpha\beta} \tau_{ij} c_{i\alpha}^\dagger (\vec{\sigma} \times \vec{d}_{ij}^{\,0})_{\alpha\beta}^z c_{j\beta} \quad (3)$$

The operator $c_{i\alpha}^\dagger (c_{i\alpha})$ is responsible for creating (annihilating) an electron with spin α at the site i and t = -1.3 eV represents the hopping energy between nearest neighbors, being zero otherwise. Summation over $\langle i, j \rangle$ and $\langle\langle i, j \rangle\rangle$ denotes the inclusion of nearest and next-nearest neighbors, respectively. In Equation (3), the second term signifies the effective spin-orbit (SO) coupling with a value of $\lambda_{SO} = 43meV$. In this equation, $\vec{\sigma} = (\sigma_x, \sigma_y, \sigma_z)$ refers to

the Pauli spin matrix. If the next-nearest neighbor hopping is in the clockwise (anticlockwise) direction relative to the positive z-axis, the parameter ν_{ij} will take a value of +1 (-1). The third term in Equation (3) describes the intrinsic Rashba interaction and involves the parameter $\lambda_{Ra} = 10.7meV$. Here, $\mu_{ij} = +1(-1)$ for A(B) sites, $\vec{d}_{ij}^{\,0} = \vec{d}_{ij} / \left|\vec{d}_{ij}\right|$, and $\vec{d}_{ij}$ represents a vector connecting *i* and *j* sites within the same sublattice [30]. The retarded Green's function $G^r(E)$ and Γ, denoting the broadening function are given by:

$$G^r(E) = [(E + i\eta)I - H_c - \Sigma_\sigma^r(E)]^{-1}$$
$$\Gamma_{L(R)}(E) = i[\Sigma_{L(R)}(E) - (\Sigma_{L(R)}A(E))^+] \quad (4)$$

The variable $\Sigma_\sigma^r(E) = \Sigma_L^r(E) + \Sigma_R^r(E)$ represents the overall self-energy, which accounts for the impact of both the left and the right electrodes. Consequently, the transmission function, denoted as T, can be determined using the following equation for the non-interacting system [31]:

$$T(E) = Tr[\Gamma_L G^r \Gamma_R (G^r)^\dagger] \quad (5)$$

The Landauer formula for a two dimensional systems (potential step scattering) can be written as [31]:

$$I = \frac{2e}{h}\int T(E)[f_L(E) - f_R(E)]dE \quad (6)$$

$f_{L(R)}$ represents the Fermi distribution function for the left and right electrodes and $f_L(E) - f_R(E) = \left[1 + exp\left(\frac{E-\mu_L}{K_BT}\right)\right]^{-1} - \left[1 + exp\left(\frac{E-\mu_R}{K_BT}\right)\right]^{-1}$ is closely associated with the temperature of the electrodes, with T_L and T_R representing the temperatures of the left and the right electrodes, respectively. Because of the disparity in Fermi distributions, carriers with energy higher than the Fermi energy flow from the higher temperature left electrode to the lower temperature right electrode, leading to both electron and phonon currents. The non-equilibrium Green's function method is employed to determine the phonon transmission $T_{ph}(\omega)$, where ω denotes the phonon frequency. Subsequently, the Landauer-Büttiker formalism is utilized to compute the quasi-ballistic thermal conductance [26]:

$$k_{ph} = \frac{k_B^2 T_0}{h}\int_0^\infty dx \frac{x^2 e^x}{(e^x - 1)^2} T_{ph}\left(\frac{k_B T_0}{\hbar}x\right) \quad (7)$$

Where k_B, h and T_0, are Boltzmann constant, Planck constant, and absolute temperature, respectively. The x function is defined as $x = \frac{\hbar\omega}{k_B T_0}$. Therefore, by having access to electronic transmission and thermal conductance, one can compute the thermoelectric properties of the junction using the following parameters [27-29]:

$$G = e^2 L_0 \quad (8)$$
$$k_e = \frac{1}{T_0}\left(L_2 - \frac{L_1^2}{L_0}\right) \quad (9)$$
$$S = -\frac{1}{eT_0}\frac{L_1}{L_0} \quad (10)$$
$$ZT = \frac{|G|S^2 T_0}{k_e + k_{ph}} \quad (11)$$

Where the transport coefficient L_n given as [32] :

$$L_n = \frac{1}{h}\int T(E)(E-\mu)^n \left[-\frac{\partial f(E)}{\partial E}\right]_{\mu,T} dE \quad (12)$$

3. Results and discussion

The band structure analysis of the armchair germanene nanoribbons revealed distinct variations in the band gaps across the different nanostructures. As seen in Figure 4, the AGeNR exhibits a complete absence of a band gap, indicating metallic behavior.

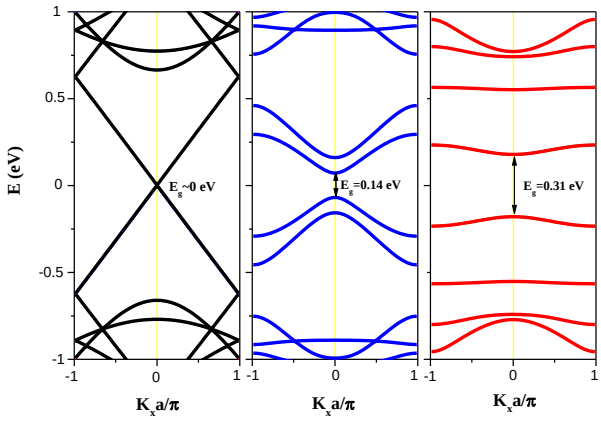

Fig. 4. Band structures of AGeNR (black curve) and AGeNMs with the symmetric (blue curve) and asymmetric (red curve) rhomboid-type quantum antidot arrays.

In contrast, the AGeNM with a symmetric rhomboid demonstrated a finite band gap of 0.14 *eV*, while the AGeNM with an asymmetric rhomboid exhibited a larger band gap of 0.31 *eV*. This disparity in band gap widths among the three nanostructures underscores the notable influence of geometric configurations on the electronic properties of germanene nanoribbons. These findings not only provide valuable insights into the fundamental relationship between nanostructure geometry and electronic behavior but also offer potential avenues for tailoring the electronic properties of germanene-based nanostructures for specific applications in nanoelectronics and nanodevices. The observed variations in the band gaps of the germanene nanoribbons have direct implications for their thermoelectric properties. The presence of different band gap widths across the nanostructures suggests distinct electronic transport behaviors, influencing the materials' thermoelectric performance. Specifically, the presence of band gaps in the nanoribbons can affect their electrical conductivity and *ZT*, potentially influencing their overall thermoelectric efficiency. Therefore, understanding and manipulating the band structure and its impact on the thermoelectric properties of these nanoribbons is crucial for optimizing their potential in thermoelectric applications.

We now aim to investigate the heat transfer properties of AGeNR and AGeNMs. Figure 5 demonstrates the phonon

thermal conductance of AGeNR and AGeNMs, where quantum antidot arrays are placed in the central region and the electrodes of the nanoribbons. When the quantum antidot arrays are created in the nanoribbon, the phonon thermal conductance quickly decreases. The phonon thermal conductance of the pristine AGeNR at T_L=300 K is about 2.26 nW/K.

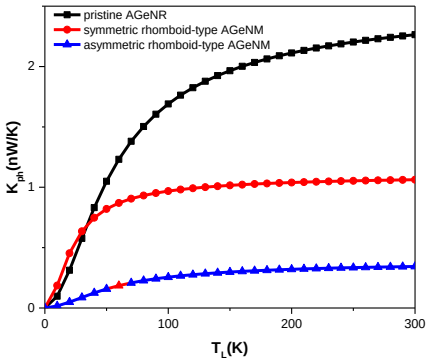

Fig. 5. Phonon thermal conductance as a function of temperature for N=11 AGeNR and two different AGeNM

The behavior of the phonon thermal conductivity curve exhibited excellent agreement with the findings presented in Yang et al. [33], indicating an increase in phonon thermal conductivity with rising temperatures. Furthermore, the asymmetric rhomboid-type AGeNM has less thermal conductance in comparison to the symmetric rhomboid-type AGeNM. For example, at T_L=300 K the phonon thermal conductance of the asymmetric rhomboid-type AGeNM is approximately 0.34 nW/K, while this value for the symmetric rhomboid-type AGeNM is about 1.06 nW/K. The curves have a similar trend as a function of temperature; however, it is obvious that for asymmetric rhomboid-type AGeNM, the reduction of k_{ph}, in comparison to pristine AGeNR, can be more than 85%. For both kinds of AGeNM, a strong reduction of k_{ph} in comparison with the pristine AGeNR can be seen in the whole temperature range. The main reason for this significant reduction is the scattering of defect-phonon. The primary factor contributing to this substantial reduction is the scattering of defect-phonons in the structures. The introduction of quantum antidot arrays in the nanoribbon leads to a rapid decrease in phonon thermal conductance. As a result, the phonon transport in AGeNR and AGeNMs is significantly hindered by the presence of defects, resulting in a lower thermal conductance overall. These findings highlight the potential for controlling and manipulating heat transport properties in AGeNR and AGeNMs by introducing quantum antidot arrays and altering the geometry of the structures. The observed reductions in thermal conductance have important implications for the design and optimization of these materials for various applications in thermoelectric devices and heat management systems.

In Figure 6, the Seebeck coefficient, the electron thermal conductance, the electric conductance, and the figure of merit of the pristine AGeNR and AGeNMs as a function of chemical potential have been shown. To calculate the quantities in our system, we assume $\mu_L = \mu_R$ =0, T_R =0K and T_L = 300K. These plots demonstrate different thermoelectric quantities for AGeNR (black lines), symmetric rhomboid-type AGeNM (red lines), and asymmetric rhomboid-type AGeNM (blue lines).

In Figure 6(a), the Seebeck coefficient of pristine AGeNR and AGeNMs can be seen. The magnitude of the main peak S value in pristine AGeNR, symmetric rhomboid-type, and asymmetric rhomboid-type AGeNM, at $\mu = 0.2eV$, is approximately 0.023 mV/K, 0.26 mV/K, and 0.57 mV/K, respectively. On the other hand, by applying quantum antidots, the Seebeck coefficient exhibits a significant increase because of breaking electron–hole symmetry and the quantum interference impacts. This point has been presented in Figure 6(a). The observed increase in the Seebeck coefficient due to the presence of quantum antidots is of great interest for thermoelectric applications. By breaking the electron-hole symmetry and inducing quantum interference, the introduction of quantum antidots leads to enhanced thermoelectric performance in AGeNMs. The asymmetric rhomboid-type AGeNM with quantum antidots exhibits the highest Seebeck coefficient, indicating its potential for efficient thermoelectric energy conversion. The higher Seebeck coefficient suggests a greater ability to generate electric voltage in response to temperature gradients, making it a promising candidate for thermoelectric devices.

In Figure 6(b) and (c), it can be seen that when quantum antidot arrays are applied, the electric conductance and the electron thermal conductance display a significant reduction in the center of the band ($\mu = 0$). For example, the electric conductance for symmetric rhomboid-type AGeNM and asymmetric rhomboid-type AGeNM reduces by about 56% and 72%, respectively, and electron thermal conductance decreases for the same by about 37% and 57%, respectively. These reductions in electric conductance and electron thermal conductance highlight the influence of quantum antidots on the transport properties of AGeNM structures. The presence of quantum antidots disrupts the flow of electrons, leading to a decrease in both electric and thermal conductivity.

In Figure 6(d), one can observe that by imposing the quantum antidot arrays in nanoribbons, the ZT value significantly increases. This increase is due to the scattering of electrons and phonons. Moreover, the magnitudes of the ZT peak in the asymmetric rhomboid-type AGeNM are higher than those of the symmetric rhomboid-type AGeNM. The increase of the ZT peak values in asymmetric rhomboid-type AGNM originates from the increase of S^2G and the reduction of thermal conductance. The scattering of phonons by the quantum antidot arrays leads to a reduction in thermal conductivity, resulting in improved energy conversion efficiency. Overall, the imposition of quantum antidot arrays in AGeNM nanoribbons offers a promising approach for enhancing the ZT value. By effectively scattering both electrons and phonons, quantum antidots contribute to the improvement of the power factor and the reduction of thermal conductance, ultimately boosting the efficiency of thermoelectric devices. These findings highlight the potential of quantum antidots as a means to optimize the thermoelectric performance of AGeNM materials, paving the way for the development of high-

efficiency thermoelectric devices for energy harvesting and waste heat recovery applications.

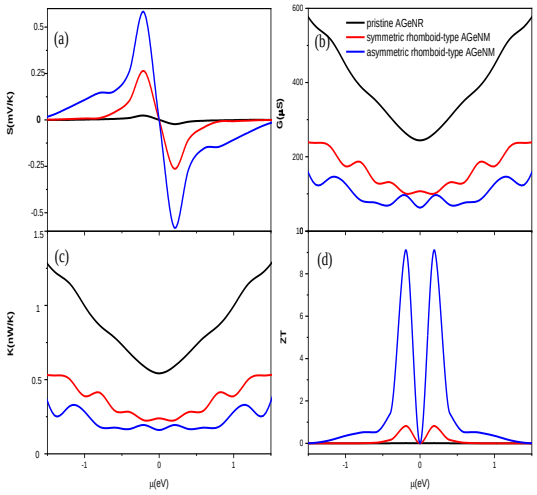

Fig. 6. (a) Seebeck coefficient, (b) Electronic conductance, (c) electron thermal conductance, (d) figure of merit and as a function of the chemical potential μ, for a fixed temperature TL = 300K. Results are shown for a N=11 AGeNR and two different AGeNM.

Several articles have reported an increase in the Seebeck coefficient and thermoelectric gain, accompanied by a decrease in electrical and thermal conductivity, as a result of defects present in nanoribbons [2, 3, 34-36]. These observations align with the findings presented in this work, demonstrate consistency with previous studies.

In Figure 7, ZT_{max} has been depicted as a function of electrode temperature. The temperature ranges from 300 *K* to 700 *K*, and the temperature of the right electrode has been considered to be T_R=0 *K*. The interesting feature of Figure 7 is that along with the temperature of the left electrode, ZT_{max} reduces uniformly. It can also be seen that the highest value of (*ZT*=9) belongs to the asymmetric rhomboid-type AGeNM at *T*=300*K* .This value is noticeable and indicates that this type of AGNM is extremely useful for thermoelectric applications. The decrease in *ZT* value with the increase in the temperature of the left electrode can be attributed to several factors. One of the primary reasons is the increase in the phonon thermal conductivity at higher temperatures. Phonons are quantum of vibrational mechanical energy of lattice that contribute to heat transfer in materials. As the left electrode temperature increases, the phonons carry more heat, resulting in higher thermal conductivity. This increased thermal conductivity leads to a decrease in the thermoelectric efficiency, causing a reduction in *ZT* value. Another reason for the decrease in *ZT* value with an increase in the temperature of the left electrode is the widening of the energy gap between the valence and conduction bands. At higher temperatures, more electrons in the valence band gain sufficient energy to transition to the conduction band, reducing the number of available charge carriers for thermoelectric processes. This decrease in charge carrier concentration further contributes to the decrease in the thermoelectric efficiency and subsequently lowers the *ZT* value. At higher temperatures, the Seebeck coefficient may decrease due to changes in the electronic band structure or scattering mechanisms, leading to a reduction in the voltage output per unit temperature difference. The reduction of the Seebeck coefficient of AGeNR and AGeNMs with increasing temperature is clearly depicted in Figure 8. This decrease in the Seebeck coefficient contributes to a decrease in the thermoelectric efficiency and subsequently lowers the overall *ZT* value. Previous studies on germanene nanoribbons have also reported a decrease in the figure of merit with increasing temperature [33-37] .

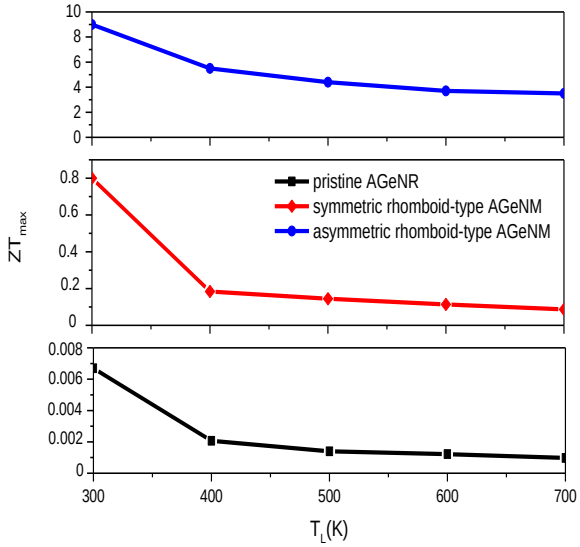

Fig. 7. Maximum figure of merit as a function of left electrode temperature (Righ electrode kept constant in TR=0 K) for a N=11 AGeNR and two different AGeNM.

The thermoelectric properties of the two rhomboid-type AGeNMs analyzed in this study exhibit significant variations. Although both systems have a similar number of extracted atoms, their thermoelectric properties manifest notable distinctions. These disparities arise not only from the absence of symmetry in the asymmetric rhomboid-type AGeNM but also from the unique geometry specific to this AGeNM type. In an asymmetric rhomboid AGeNM, the distance between the quantum antidots and the nanoribbon edges is shorter than in a symmetric rhomboid AGeNM.

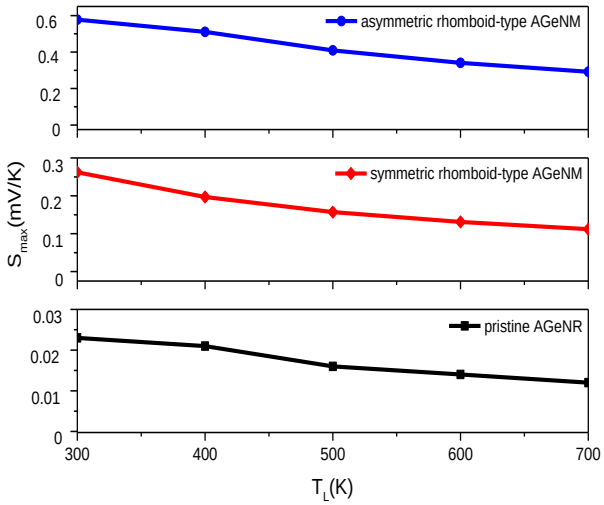

Fig. 8. Maximum Seebeck coefficient as a function of left electrode temperature (Righ electrode kept constant in T_R=0 K) for a N=11 AGeNR and two different AGeNM.

4. Conclusions

In this study, we examined the thermoelectric properties of pristine armchair germanene nanoribbons (AGeNR) and germanene nanoribbons defected by quantum antidot arrays with symmetric and asymmetric rhombus shapes (AGeNMs). For these nanoribbons, we obtained the phonon and electron thermal conductance, the electric conductance, the Seebeck coefficient, and the figure of merit. Applying quantum antidots increased the scattering of phonon-defect. Hence, there was a significant decrease in the phonon thermal conductance across a wide temperature range. Furthermore, imposing quantum antidot arrays resulted in breaking electron–hole symmetry and the quantum interference impacts. As a consequence, the Seebeck coefficient increased. The effect of left electrode temperature on the figure of merit in these nanoribbons was also investigated in this study. It was shown that the best temperature to have an appropriate figure of merit for the given nanoribbons is 300K (T_L=300K). The results also showed that the highest value of *ZT* belongs to asymmetric rhomboid AGeNM. This finding indicates that AGeNMs, especially in asymmetric rhomboid type, can be promising for thermoelectric applications.

Acknowledgements

There is nothing to acknowledgement.

Conflicts of Interest

The author declares that there is no conflict of interest regarding the publication of this article.

References

[1] Rahman, M.H., Chowdhury, E.H., Redwan, D.A. and Hong, S., 2021. Computational characterization of thermal and mechanical properties of single and bilayer germanene nanoribbon. *Computational Materials Science*, *190*, p.110272.

[2] Kalami, R. and Ketabi, S.A., 2023. Role of Linear Defects on the Electronic, Transport, and Thermoelectric Properties of Armchair Edge Silicene Nanoribbons. *Journal of Electronic Materials*, pp.1-11.

[3] Kalami, R. and Ketabi, S.A., 2023. Electronic and Thermoelectric Properties of Armchair-Edge Silicene Nanoribbons: Role of Quantum Antidot Arrays. *Journal of Electronic Materials*, *52*(10), pp.6566-6577.

[4] Shokri, A. and Salami, N., 2019. Thermoelectric properties in monolayer MoS 2 nanoribbons with Rashba spin–orbit interaction. *Journal of Materials Science*, *54*(1), pp.467-482.

[5] Checkelsky, J.G. and Ong, N.P., 2009. Thermopower and Nernst effect in graphene in a magnetic field. *Physical Review B*, *80*(8), p.081413.

[6] Yan, Y., Liang, Q.F., Zhao, H., Wu, C.Q. and Li, B., 2012. Thermoelectric properties of one-dimensional graphene antidot arrays. *Physics Letters A*, *376*(35), pp.2425-2429.

[7] Domínguez-Adame, F., Martín-González, M., Sánchez, D. and Cantarero, A., 2019. Nanowires: A route to efficient thermoelectric devices. *Physica E: Low-dimensional Systems and Nanostructures*, *113*, pp.213-225.

[8] Núñez, C., Saiz-Bretín, M., Orellana, P.A., Rosales, L. and Domínguez-Adame, F., 2020. Tuning the thermoelectric response of silicene nanoribbons with vacancies. *Journal of Physics: Condensed Matter*, *32*(27), p.275301.

[9] Gayner, C. and Kar, K.K., 2016. Recent advances in thermoelectric materials. *Progress in Materials Science*, *83*, pp.330-382.

[10] Yu, C., Shi, L., Yao, Z., Li, D. and Majumdar, A., 2005. Thermal conductance and thermopower of an individual single-wall carbon nanotube. *Nano letters*, *5*(9), pp.1842-1846.

[11] Sadeghi, H., Sangtarash, S. and Lambert, C.J., 2015. Enhancing the thermoelectric figure of merit in engineered graphene nanoribbons. *Beilstein journal of nanotechnology*, *6*(1), pp.1176-1182.

[12] Ouyang, Y. and Guo, J., 2009. A theoretical study on thermoelectric properties of graphene nanoribbons. *Applied Physics Letters*, *94*(26).

[13] Ni, X., Liang, G., Wang, J.S. and Li, B., 2009. Disorder enhances thermoelectric figure of merit in armchair graphane nanoribbons. *Applied Physics Letters*, *95*(19).

[14] Chen, Y., Jayasekera, T., Calzolari, A., Kim, K.W. and Nardelli, M.B., 2010. Thermoelectric properties of graphene nanoribbons, junctions and superlattices. *Journal of Physics: Condensed Matter*, *22*(37), p.372202.

[15] Yu, J.K., Mitrovic, S., Tham, D., Varghese, J. and Heath, J.R., 2010. Reduction of thermal conductivity in phononic nanomesh structures. *Nature nanotechnology*, *5*(10), pp.718-721.

[16] Markussen, T., Jauho, A.P. and Brandbyge, M., 2009. Electron and phonon transport in silicon nanowires: Atomistic approach to thermoelectric properties. *Physical Review B*, *79*(3), p.035415.

[17] Liu, L. and Chen, X., 2010. Effect of surface roughness on thermal conductivity of silicon nanowires. *Journal of Applied Physics*, *107*(3).

[18] Pan, L., Liu, H.J., Tan, X.J., Lv, H.Y., Shi, J., Tang, X.F. and Zheng, G., 2012. Thermoelectric properties of armchair and zigzag silicene nanoribbons. *Physical Chemistry Chemical Physics*, *14*(39), pp.13588-13593.

[19] Pop, E., Varshney, V. and Roy, A.K., 2012. Thermal properties of graphene: Fundamentals and applications. *MRS bulletin*, *37*(12), pp.1273-1281.

[20] Saiz-Bretín, M., Malyshev, A.V., Domínguez-Adame, F., Quigley, D. and Römer, R.A., 2018. Lattice thermal conductivity of graphene nanostructures. *Carbon*, *127*, pp.64-69.

[21] Nouri, N., Rashedi, G. and Karbaschi, H., 2020. Analysis of electronical properties of Bismuth and Silicene antidot in the presence of strain using the four-orbital tight-binding method. *Physics Letters A*, *384*(17), p.126364.

[22] Kim, M., Safron, N.S., Han, E., Arnold, M.S. and Gopalan, P., 2010. Fabrication and characterization of large-area, semiconducting nanoperforated graphene materials. *Nano letters*, *10*(4), pp.1125-1131.

[23] Bai, J., Zhong, X., Jiang, S., Huang, Y. and Duan, X., 2010. Graphene nanomesh. *Nature nanotechnology*, *5*(3), pp.190-194.

[24] Matthes, L., Pulci, O. and Bechstedt, F., 2014. Optical properties of two-dimensional honeycomb crystals graphene, silicene, germanene, and tinene from first principles. *New Journal of Physics*, *16*(10), p.105007.
[25] Samipour, A., Dideban, D. and Heidari, H., 2020. Impact of an antidote vacancy on the electronic and transport properties of germanene nanoribbons: A first principles study. *Journal of Physics and Chemistry of Solids*, *138*, p.109289.
[26] Shirdel-Havar, M. and Farghadan, R., 2018. Spin caloritronics in spin semiconducting armchair graphene nanoribbons. *Physical Review B*, *97*(23), p.235421.
[27] Goharrizi, A.Y., Pourfath, M., Fathipour, M. and Kosina, H., 2012. Device performance of graphene nanoribbon field-effect transistors in the presence of line-edge roughness. *IEEE Transactions on electron devices*, *59*(12), pp.3527-3532.
[28] Klimeck, G., Ahmed, S.S., Bae, H., Kharche, N., Clark, S., Haley, B., Lee, S., Naumov, M., Ryu, H., Saied, F. and Prada, M., 2007. Atomistic simulation of realistically sized nanodevices using NEMO 3-D—Part I: Models and benchmarks. *IEEE Transactions on Electron Devices*, *54*(9), pp.2079-2089.
[29] Klimeck, G., Ahmed, S.S., Bae, H., Kharche, N., Clark, S., Haley, B., Lee, S., Naumov, M., Ryu, H., Saied, F. and Prada, M., 2007. Atomistic simulation of realistically sized nanodevices using NEMO 3-D—Part I: Models and benchmarks. *IEEE Transactions on Electron Devices*, *54*(9), pp.2079-2089.
[30] Liu, C.C., Jiang, H. and Yao, Y., 2011. Low-energy effective Hamiltonian involving spin-orbit coupling in silicene and two-dimensional germanium and tin. *Physical Review B*, *84*(19), p.195430.
[31] Datta, S., 1997. *Electronic transport in mesoscopic systems*. Cambridge university press.
[32] Kalami, R. and Ketabi, S.A., 2021. Spin-dependent thermoelectric properties of a magnetized zigzag graphene nanoribbon. *Progress in Physics of Applied Materials*, *1*(1), pp.1-6.
[33] Yang, K., Cahangirov, S., Cantarero, A., Rubio, A. and D'Agosta, R., 2014. Thermoelectric properties of atomically thin silicene and germanene nanostructures. *Physical Review B*, *89*(12), p.125403
[34] Banoozadeh, B., Pilevar Shahri, R., Benam, M., Baedi, J. and Kafi, F., 2022. Theoretical investigation and comparison of thermoelectric properties of porous and perfect phosphorene along armchair direction. *Journal of Research on Many-body Systems*, *12*(2), pp.9-19.
[35] Gholami, Z. and Khoeini, F., 2021. Vacancy tuned thermoelectric properties and high spin filtering performance in graphene/silicene heterostructures. *Scientific Reports*, *11*(1), p.15320.
[36] Peng, Y.N., Yu, J.F., Cao, X.H., Wu, D., Jia, P.Z., Zhou, W.X. and Chen, K.Q., 2020. An efficient mechanism for enhancing the thermoelectricity of twin graphene nanoribbons by introducing defects. *Physica E: Low-dimensional Systems and Nanostructures*, *122*, p.114160.
[37] Banerjee, L., Sengupta, A. and Rahaman, H., 2018. Carrier transport and thermoelectric properties of differently shaped germanene (Ge) and silicene (Si) nanoribbon interconnects. *IEEE Transactions on Electron Devices*, *66*(1), pp.664-669.